

# Non-perturbative calculations of nuclear matter using in-medium similarity renormalization group

Xin Zhen,<sup>1</sup> Rongzhe Hu,<sup>1</sup> Haoyu Shang,<sup>1</sup> Jiawei Chen,<sup>1</sup> J.C. Pei,<sup>1,2,\*</sup> and F.R. Xu<sup>1,2</sup>

<sup>1</sup>State Key Laboratory of Nuclear Physics and Technology,  
School of Physics, Peking University, Beijing 100871, China

<sup>2</sup>Southern Center for Nuclear-Science Theory (SCNT),  
Institute of Modern Physics, Chinese Academy of Sciences, Huizhou 516000, China

The non-perturbative *ab initio* calculations of infinite nuclear matter using In-Medium Similarity Renormalization Group (IMSRG) method is developed in this work, which enables calculations with chiral two and three-nucleon forces at N<sup>2</sup>LO and N<sup>3</sup>LO. Results from the many-body perturbation theory at different orders and coupled-cluster theory are also presented for comparison. It is shown that different many-body approaches lead to divergences with a harder nuclear interaction for pure neutron matter. For symmetric nuclear matter, such divergences would appear even with soft nuclear interactions. This work provides a novel alternative infrastructure for future studies of dense nuclear matter and strongly-correlated many-body systems.

## I. INTRODUCTION

The homogeneous nuclear matter is a non-trivial strongly-correlated many-body system. The studies of infinite nuclear matter is particularly attractive in studies of neutron stars in the era of gravitational-wave astronomy. Indeed, the multi-messenger astrophysics studies of neutron stars provide unique opportunities for constraining the properties of dense nuclear matter [1–8]. In particular, the recent observations of a massive neutron star of 2.35 solar mass brought a theoretical challenge [9], which means the appearance of exotic structures in speed of sound and equation of state (EoS) around two times of nuclear saturation density ( $\rho_{\text{sat}}$ ) [10]. At extremely high densities above  $40\rho_{\text{sat}}$ , the strongly interacting matter can be calculated by the perturbative QCD [11]. The progress in reliable *ab initio* calculations of nuclear EoS at intermediate densities is also essential for better inferences of the first-order phase transition from nuclear matter to quark matter.

The EoS of nuclear matter around the saturation density is largely known from finite nuclear properties, which can be well described by density functional theory based on phenomenological nuclear forces. It is still of fundamental interests to describe nuclear matter above the saturation density with realistic nuclear interactions and *ab initio* many-body methods. In this respect, the development of modern two-nucleon and three-nucleon interactions from chiral effective field (EFT) provided a consistent theory of nuclear forces rooted in chiral-symmetry breaking of QCD [12–14]. Advanced *ab initio* calculations based on chiral nuclear forces have been very successful in descriptions of finite nuclear properties [15–18], which can be naturally applied to infinite nuclear matter.

There have been a variety of *ab initio* methods for studies of nuclear matter. For example, the many-body perturbation theory (MBPT) has been extensively applied in

a series of works [19–21] to calculate EoS of pure neutron matter and symmetric nuclear matter. The MBPT calculations have been developed up to MBPT4 at 4th order in the momentum space [20]. In addition, the coupled-cluster (CC) theory, which is a non-perturbative method using non-unitary transformations on Hamiltonian has been applied in studies of nuclear matter [22, 23]. The Green function method and Monte Carlo method have also been applied to nuclear matter [24–28]. Most of these many-body methods are regarded as post-Hartree-Fock methods to incorporate higher correlations beyond the mean field approximation.

It is expected that non-perturbative calculations are important for strongly-correlated nuclear matter, particularly, at higher densities. The purpose of this work is to study nuclear matter from first principles using the In-Medium Similarity Renormalization Group (IMSRG) method. IMSRG is a novel non-perturbative many-body method, which incorporates many-body correlations efficiently via unitary transformations on the many-body Hamiltonian [29, 30]. Actually IMSRG provides an alternative non-perturbative method in truncations of many-body operators compared to the coupled-cluster theory. IMSRG(2) refers to the scheme that all operators are truncated at the normal-ordered two-body level although three-body forces are invoked. IMSRG(3) is truncated at the normal-ordered three-body level but it is computationally very costly [32, 33, 41]. The coupled-cluster calculations are usually truncated at the CCSD level that includes single and double particle-hole excitations. The IMSRG method has been used in *ab initio* calculations of finite nuclei in recent years [16, 17, 30], but it has not been applied in studies of nuclear matter yet.

## II. METHODS

In this section, we introduce how to implement the IMSRG calculations in momentum spaces based on chiral

\* peij@pku.edu.cn

nuclear forces.

### A. Magnus IMSRG(2)

Firstly, IMSRG is based on a unitary flow transformation [29, 30] in which the eigenvalue of an operator remains unchanged.

$$H(s) = U(s)H(0)U^\dagger(s). \quad (1)$$

Here the transformation is continuous and  $s$  is the flow parameter. One can choose a specific  $U$  to obtain a transformed Hamiltonian whose off-diagonal part is as small as possible so that we can solve it in a reduced space. The derivative of  $H(s)$  should be

$$\frac{d}{ds}H(s) = [\eta(s), H(s)], \quad (2)$$

where  $\eta(s)$  is defined as the generator and is related to  $U$  as

$$\eta(s) \equiv \frac{dU(s)}{ds}U^\dagger(s) = -\eta^\dagger(s). \quad (3)$$

The generator is anti-Hermitian because of the Hermiticity of  $U$ . The unitary transformation can be determined by choosing a generator. The choice of generator  $\eta$  depends on which part of Hamiltonian is chosen to be diagonal. There are different possible types of generators, and we have adopted the White generator [30] in this work. It can be written as

$$\eta^{\text{White}} = \frac{H^{\text{od}}}{\Delta}. \quad (4)$$

Here  $H^{\text{od}}$  is the off-diagonal part we choose, and  $\Delta$  is a denominator related to energies. The denominator could be chosen by different energy partitioning such as the Møller-Plesset scheme, and the Epstein-Nesbet scheme which we used in this work. Following Ref. [30], the two-body part of White generator is written as an instance:

$$\eta_{pp'hh'} \equiv \frac{\Gamma_{pp'hh'}}{f_{p'} + f_p - f_{h'} - f_h - A_{pp'hh'}}, \quad (5)$$

$$A_{pp'hh'} = \Gamma_{pp'pp'} + \Gamma_{hh'hh'} - \Gamma_{phph} - \Gamma_{p'h'p'h'} - \Gamma_{ph'ph'} - \Gamma_{p'h'p'h}. \quad (6)$$

Here  $p$  and  $h$  denote particle states and hole states, which are above or below the Fermi momentum, respectively. The particle-particle hole-hole configurations are the off-diagonal part. The two-body interaction matrix after normal-ordering  $\Gamma$  is explicitly suppressed by (5) during the flow evolution.

The IMSRG evolution is a first-order operator differential equation. In order to get precise and stable numerical results, Magnus expansion has been introduced in solving IMSRG equations [31]. One can rewrite  $U$  as

$$U(s) = e^{\Omega(s)}. \quad (7)$$

By applying the Baker-Campbell-Hausdorff formula, we can get the evolution of  $\Omega(s)$  as

$$\frac{d}{ds}\Omega(s) = \sum_{k=0}^{\infty} \frac{B_k}{k!} [\Omega(s), \eta(s)]^{(k)}. \quad (8)$$

Here  $B_k$  is the  $k$ -th Bernoulli number and the  $k$ -order nested commutator is defined as

$$[\Omega(s), \eta(s)]^{(k)} = \begin{cases} \eta(s), & \text{if } k = 0, \\ [\Omega(s), [\Omega(s), \eta(s)]^{(k-1)}], & \text{if } k > 0. \end{cases} \quad (9)$$

Therefore, the transformation of Hamiltonian is written as

$$H(s) = e^{\Omega(s)}H(0)e^{-\Omega(s)} = \sum_{k=0}^{\infty} \frac{1}{k!} [\Omega(s), H(0)]^{(k)}. \quad (10)$$

Based on this framework, one can perform calculations of the ground state energy of a many-body system non-perturbatively. It has been pointed out that IMSRG could be regarded as kind of summation of MBPT diagrams to infinite order [30]. This means that IMSRG is a non-perturbative method and could invoke more correlations than MBPT when configuration space is fixed, which is important as the density increases.

A many-body operator could be given in second-quantized form as

$$O = \sum_{pq} T_{pq} a_p^\dagger a_q + \frac{1}{2!} \sum_{pqrs} V_{pqrs} a_p^\dagger a_q^\dagger a_s a_r + \frac{1}{3!} \sum_{pqrst} W_{pqrst} a_p^\dagger a_q^\dagger a_r^\dagger a_u a_t a_s + \dots \quad (11)$$

In the flow equation, there are commutators of operators which may induce higher-order many-body terms beyond the original Hamiltonian. For instance, the commutation between two-body operators can induce three-body operators.

$$[A^{(2)}, B^{(2)}] = C^{(0)} + C^{(1)} + C^{(2)} + C^{(3)}. \quad (12)$$

The induced three-body terms can subsequently induce growing many-body terms beyond three-body terms, which means the unitary flow evolution would ultimately contain A-body operators. Usually, we make a truncation on the flow equation, by dropping all terms higher than a specific order. If we drop  $C^{(3)}$  and all induced terms higher than two-body operators, the scheme is called IMSRG(2). The terms with three-body forces are truncated at the normal-ordered two-body level. Fortunately the unitary transformations is almost kept with the truncation. There have been efforts to take back some induced terms that are dropped to improve IMSRG results [32, 33].

### B. Interactions in Momentum Space

For calculations of nuclear matter, it is a natural choice to use plane wave basis with the periodic boundary condition. One can adopt discretized momentum within a

cubic box [23]. Instead, we adopt a sphere in the momentum space to calculate the infinite matter. The number of nucleons is determined by the lattice points within a definite Fermi sphere. The number of nucleons is given by:

$$A = g_s g_t N. \quad (13)$$

Here  $g_s, g_t$  reflects the spin-isospin degeneracy and  $g_s g_t$  is 4 for SNM and 2 for PNM.  $N = 1, 7, 19, 27, 33, \dots$  denotes lattice points within the sphere. The lattice spacing is determined by the density in calculations, which is similar to Ref.[23]. There could be finite-size effect due to a finite box. Nevertheless, the finite-size corrections decrease rapidly with increasing the number of particles [23].

The hole-particle definition and normal-order procedure are both related to the Fermi sphere. As the first-order calculation of IMSRG, the Hartree-Fock (HF) energy in plane wave basis is given by summation as

$$E^{\text{HF}} = \frac{1}{2} \sum_{i,j} V_{ijij} n_i n_j, \quad (14)$$

where  $n_j$  is the occupation number that equals 1 for holes and 0 for particles. Afterwards, higher-order correlation energies can be calculated by invoking sufficient particle states beyond Fermi sphere until the convergence is reached. In this work, we mainly adopt  $N = 33$ , corresponding to 4 shells in momentum spaces for neutron matter. Such a choice of  $N$  parameter has been used in earlier works [23, 28] and we also tested it considering the convergence.

Once we built the basis wave functions, we can write down the interaction matrix elements in momentum space. In most studies, chiral forces are fitted to nucleon-nucleon scattering experiments, and it is convenient to write the operators in  $LSJ$  angular momentum representation. In some versions of chiral forces, regulators could be different for each partial wave [34–36]. It is complicated to perform transformation from the  $LSJ$  representation into the plane wave representation. In this work, the interaction matrix is written in the plane wave basis directly considering different regulators. This has been benchmarked with calculations in  $LSJ$  representation.

Generally, the chiral  $NN$  forces could be written as [14]:

$$\begin{aligned} V_{NN} &= \mathcal{V}_C + \mathcal{V}_S \boldsymbol{\sigma}_1 \cdot \boldsymbol{\sigma}_2 + \mathcal{V}_T (\boldsymbol{\sigma}_1 \cdot \mathbf{q})(\boldsymbol{\sigma}_2 \cdot \mathbf{q}) \\ &+ \mathcal{V}_{T,k} (\boldsymbol{\sigma}_1 \cdot \mathbf{k})(\boldsymbol{\sigma}_2 \cdot \mathbf{k}) + \mathcal{V}_{LS} (-i) \mathbf{S} \cdot (\mathbf{q} \times \mathbf{k}) \\ &+ \mathcal{V}_{\sigma L} [\boldsymbol{\sigma}_1 \cdot (\mathbf{q} \times \mathbf{k})][\boldsymbol{\sigma}_2 \cdot (\mathbf{q} \times \mathbf{k})]. \end{aligned} \quad (15)$$

Here  $\mathbf{q}$  and  $\mathbf{k}$  are related to momentum of in-state and out-state. The coefficients are defined by:

$$V_i = V_i^{\text{cont}} + (V_i + \boldsymbol{\tau}_1 \cdot \boldsymbol{\tau}_2 W_i). \quad (16)$$

The emergence of three-body chiral interactions begins at N<sup>2</sup>LO in chiral EFT and it is vital for nuclear matter

calculation. It is known that the inclusion of 3N force is essential for reasonable descriptions of saturation properties of symmetric nuclear matter [37, 38]. The 3N force at N<sup>2</sup>LO includes three terms:

$$V_E = \frac{c_E}{f_\pi^4 \Lambda_\chi} \frac{1}{2} \sum_{i \neq j} \boldsymbol{\tau}_i \cdot \boldsymbol{\tau}_j, \quad (17)$$

$$V_D = -\frac{c_D}{f_\pi^2 \Lambda_\chi} \frac{g_A^2}{8f_\pi^2} \sum_{i \neq j \neq k} \frac{(\boldsymbol{\sigma}_i \cdot \mathbf{q}_j)(\boldsymbol{\sigma}_j \cdot \mathbf{q}_i)(\boldsymbol{\tau}_i \cdot \boldsymbol{\tau}_j)}{q_j^2 + m_\pi^2}, \quad (18)$$

$$V_C = \frac{g_A^2}{8f_\pi^2} \sum_{i \neq j \neq k} \frac{(\boldsymbol{\sigma}_i \cdot \mathbf{q}_i)(\boldsymbol{\sigma}_k \cdot \mathbf{q}_k)}{(q_i^2 + m_\pi^2)(q_k^2 + m_\pi^2)} F_{ijk}. \quad (19)$$

$$\begin{aligned} F_{ijk} &= \left( -\frac{4c_1 m_\pi^2}{f_\pi^2} + \frac{2c_3}{f_\pi^2} \mathbf{q}_i \cdot \mathbf{q}_k \right) \boldsymbol{\tau}_i \cdot \boldsymbol{\tau}_k \\ &+ \frac{c_4}{f_\pi^2} (\boldsymbol{\tau}_i \times \boldsymbol{\tau}_k) \cdot \boldsymbol{\tau}_j (\mathbf{q}_i \times \mathbf{q}_k) \cdot \boldsymbol{\sigma}_j. \end{aligned}$$

In 3N chiral forces,  $f_\pi$ ,  $m_\pi$ ,  $g_A$  and the breakdown scale of chiral EFT  $\Lambda_\chi = 700 \sim 800$  MeV are fixed physical constants. The parameters  $c_D$ ,  $c_E$  have to be determined by calculations of finite nuclei. The parameters  $c_1$ ,  $c_3$  and  $c_4$  are constructed consistently with N<sup>2</sup>LO two-body forces. In this work we adopt  $\Lambda_\chi = 800$  MeV and the  $c_D$ ,  $c_E$  parameters are taken from earlier works [23, 34], .

In practical calculations, one should apply regulators on the bare nuclear interactions. In addition,  $NN$  interactions should multiply a relativity factor. The detailed expressions of chiral interactions can be found in [18, 35, 36]. There are different types of regulators and in this work, the conventional local and nonlocal regulators are employed. The expressions of regulators are given in the later part of this work. Note that the choice of regulators can impact calculated EoS of nuclear matter at high densities [23].

### C. Decomposition and Normal-Order

The interaction matrix elements can be calculated by performing complex matrix products. To improve both the speed and accuracy of our calculations, we use automatic partial-wave decomposition (aPWD) technique [39, 40] as a numerical treatment of chiral nuclear forces. In aPWD, all potential terms are separated into coefficients and operators. The expectation values of operators can be calculated in advance. As an example, for the spin-spin operator  $\boldsymbol{\sigma}_1 \cdot \boldsymbol{\sigma}_2$ , the whole spin space is the direct product of the spin spaces of two particles. Therefore, for two spin-up particles, the  $\sigma_{1x} \sigma_{2x}$  component can be calculated as

$$(\langle \uparrow | \otimes \langle \uparrow |) (\sigma_x \otimes \sigma_x) (| \uparrow \rangle \otimes | \uparrow \rangle) = 0. \quad (20)$$

For combinations of quantum numbers, all possible values of an operator can be estimated efficiently by the decomposition. Using this technique, the direct matrix calculations are transformed into case selections in our code, so that calculations become much faster. We have separated spin and isospin spaces and finally we obtain four types of decomposition in advance:

$$\boldsymbol{\sigma}_1 \cdot \boldsymbol{\sigma}_2, \boldsymbol{\sigma} \cdot \boldsymbol{v}, (\boldsymbol{\sigma}_1 + \boldsymbol{\sigma}_2) \cdot \boldsymbol{v}, (\boldsymbol{\tau}_1 \times \boldsymbol{\tau}_2) \cdot \boldsymbol{\tau}_3. \quad (21)$$

Here  $\boldsymbol{\sigma}$  and  $\boldsymbol{\tau}$  are Pauli matrices and  $\boldsymbol{v}$  is a casual vector. These four kinds of terms cover all operator structures associated with  $NN$  and  $3N$  interactions.

Presently, the operators related to three-body forces are truncated at the normal-ordered two-body level. The full three-body matrix elements are at the scale of  $N^6$ , compared to  $N^4$  for two-body forces. The treatment of residual three-body forces is a demanding task. Recently IMSRG(3) has been realized for calculations of some light nuclei [41]. The normal-ordered two-body Hamiltonian is written as

$$\tilde{V}_{pqrs} = V_{pqrs} + \sum_{i,j} W_{pqirsj} n_i n_j \delta_{ij}. \quad (22)$$

Here  $V$  denotes the original two-body interaction element and  $W$  denotes the three-body interaction element, as  $\delta$  is the Kronecker symbol. The expression of zero-body and one-body normal-ordered Hamiltonian also have similar expressions, but have different coefficients [38, 42]. Finally all elements are constructed to be anti-symmetrized.

#### D. Other Many-Body Methods

In addition to IMSRG(2), we have built other many-body methods to calculate EoS of nuclear matter for benchmark and comparison purposes. We have calculated MBPT energy to the 4th order, and the coupled-cluster method is truncated at CCD including double excitations. All these three methods are based on HF energy as a start.

In MBPT2, the correlation energy beyond HF could be expressed as

$$E^{\text{MBPT2}} = \frac{1}{4} \sum_{i,j,a,b} \frac{V_{ijab} V_{abij}}{\epsilon_{ij}^{ab}} n_i n_j (1 - n_a)(1 - n_b). \quad (23)$$

The denominator is defined as

$$\epsilon_{ij}^{ab} = \epsilon_i + \epsilon_j - \epsilon_a - \epsilon_b, \quad (24)$$

where  $\epsilon$  stands for the HF single-particle energy. The MBPT2 correlation energy can be expressed diagrammatically by one Hugenholtz diagram and the MBPT3 energy contains three diagrams. Actually, the number of diagrams increases rapidly at higher orders and

brings a challenge in MBPT calculations [38, 42, 43]. For example, there are 39 two-body Hugenholtz diagrams in MBPT4. As mentioned before, IMSRG is non-perturbative and has the capability to sum over diagrams in MBPT to infinite orders. MBPT2 is the summation of particle-particle hole-hole elements. In IMSRG(2) evolutions, MBPT2 can be seen as the off-diagonal part of IMSRG(2), reflecting how the suppression and evolution have been achieved.

Another method we use, CC, is also non-perturbative. In contrast to the unitary transformation in IMSRG, CC performs a non-unitary transformation and the evolved Hamiltonian is upper triangular, while the IMSRG Hamiltonian is block diagonal. The analytical formalism of double-excited coupled cluster (CCD) equation can be found in related literatures [23, 42, 44]. Since IMSRG relies on unitary transformations, it is convenient to obtain many-body wave functions for future calculations.

### III. RESULTS

We have built up our program with Fortran 90 from scratch and employed OpenMP for parallel computations. Currently our code enables calculations of nuclear matter using MBPT, CCD and IMSRG(2).

#### A. Pure Neutron Matter

Firstly, it is necessary to benchmark our code with existing calculations. In Fig. 1, the energy per particle of neutron matter are calculated with Minnesota and chiral potentials. Minnesota potential [45] has a simple form with components like spin-spin and isospin-isospin interactions and it is convenient for benchmark calculations. In our calculations, the number of nucleons are taken as  $A = 66$  for neutron matter and  $A = 76$  for symmetric matter. With the Minnesota potential, our IMSRG(2) results agree well with the CCD results in Ref.[23]. The NNLOopt potential [34] with a cutoff of 500 MeV has also been adopted in our calculations. With NNLOopt, the CCD calculations with the ladder approximation [22] are also benchmarked with Ref.[23], as shown in Fig. 1.

In Fig.2, the energy per particle from IMSRG(2) calculations with NNLOopt are compared with that from different many-body methods. The results are shown up to  $0.28 \text{ fm}^{-3}$ . Generally, IMSRG(2) results are very close to CCD results. The Hartree-Fock and CCD methods have also been benchmarked, as shown in the subfigure. In the intermediate density region below  $0.2 \text{ fm}^{-3}$ , the MBPT3 results are close to that of configuration-interaction Monte Carlo (CIMC)[25]. In the low density region below  $0.04 \text{ fm}^{-3}$ , results from different methods are close. In the high density region above  $0.23 \text{ fm}^{-3}$ , MBPT3 becomes closer to IMSRG(2) and CCD. This can be understood that NNLOopt potential is a soft interaction.

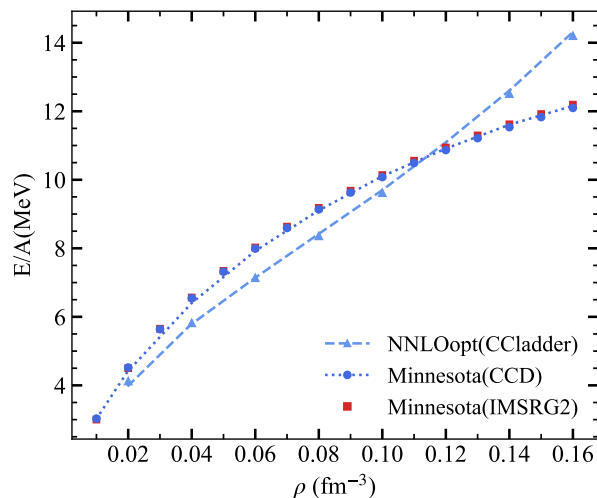


FIG. 1. Calculated energy per particle of pure neutron matter using Minnesota and NNLOopt potentials for benchmarks. Dashed lines denote results in [23].

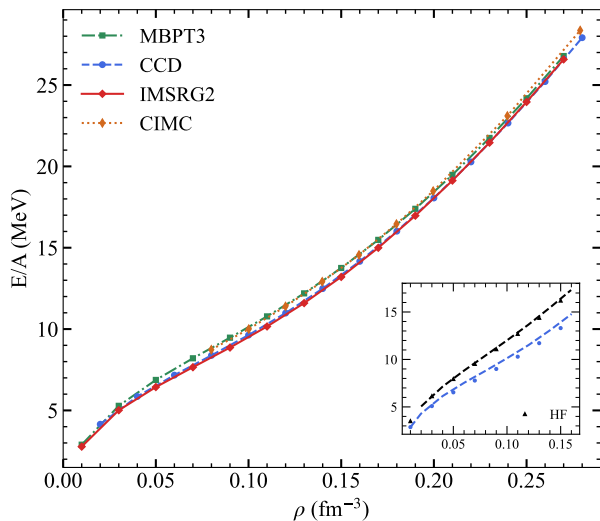


FIG. 2. Calculated energy per particle of pure neutron matter using NNLOopt. Results from MBPT3, CCD and IMSRG(2), and CIMC from [25] are compared. The subfigure shows HF and CCD benchmarks with [23].

It is interesting to compare perturbative and non-perturbative many-body calculations with a harder nuclear interaction. In chiral nuclear forces, a higher cutoff usually results in a harder interaction. In this case, the higher-order many-body correlations are non-negligible and non-perturbative calculations are needed. In Fig.3, the energy per particle based on NNLOopt with a cutoff of 500 MeV and  $N^3$ LO with a cutoff of 700 MeV are shown. We see that with NNLOopt, MBPT4 results are very close to IMSRG(2), while MBPT3 is slightly different from MBPT4. For  $N^3$ LO with a cutoff of 700 MeV [46], the results from different methods have signif-

icant discrepancies. It can be seen that MBPT4 results are relatively close to IMSRG(2) at densities below  $0.2 \text{ fm}^{-3}$ .

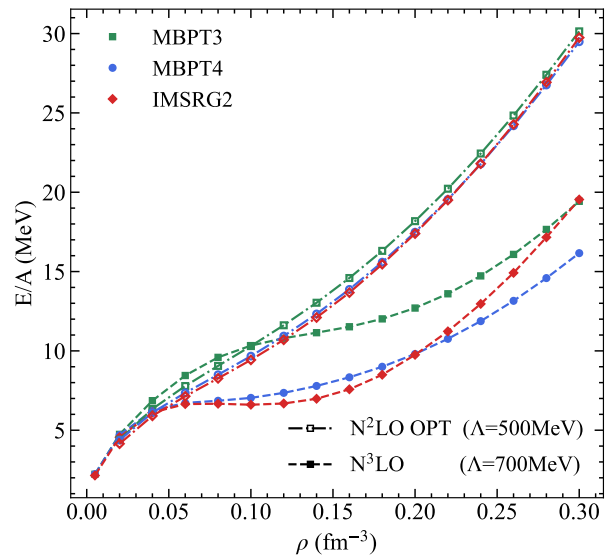


FIG. 3. Calculated energy per particle of pure neutron matter using chiral forces with different cutoffs. Results from MBPT3, MBPT4 and IMSRG(2) are compared. The  $N^3$ LO force with a cutoff of 700 MeV is from Ref.[46].

Three-body nuclear forces are crucial for calculations of nuclear matter. In this work, we adopted NNLOopt two-nucleon interactions plus three-body interactions that are normal-ordered to two-body level. For three-body forces, the regulators have both local and nonlocal formalism [23, 34]. The nonlocal regulator is written as,

$$f_{\text{nonlocal}} = \exp \left[ - \left( \frac{4p^2 + 3q^2}{\Lambda_{3N}^2} \right)^n \right]. \quad (25)$$

Here the variable  $p$  and  $q$  denote the magnitude of Jacobi momentum of a given three-body state. For the nonlocal regulator with a cutoff of 500 MeV, we adopt  $c_D = -2$  and  $c_E = -0.791$  [23]. The energy per particle of neutron matter are calculated with different methods including three-body forces, as shown in Fig.4. With the same nuclear interaction, the results from CCD calculations are benchmarked, as shown in the subfigure. It can be seen that results from different many-body methods are generally close up to densities at  $0.30 \text{ fm}^{-3}$ . IMSRG(2) results agree very well with CCD. The energies from MBPT3 is slightly above that from other two methods. With three-body forces, the EoS of neutron matter becomes harder than that with only two-body forces in Fig.2.

To study the dependence of regulators on the EoS of neutron matter, the energy per particle are calculated with both local and nonlocal regulators on three-body forces, as shown in FIG.5. The same two-body force NNLOopt is employed and the three-body forces are de-

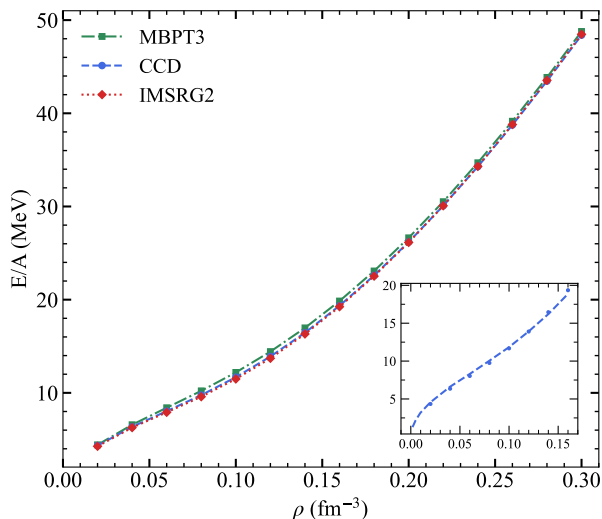


FIG. 4. Calculated energy per particle of pure neutron matter using NNLOopt plus local 3N interactions ( $\Lambda=500\text{MeV}$ ). Results from MBPT3, CCD and IMSRG(2) are compared. The subfigure shows the CCD calculations with three-body forces benchmarked with [23].

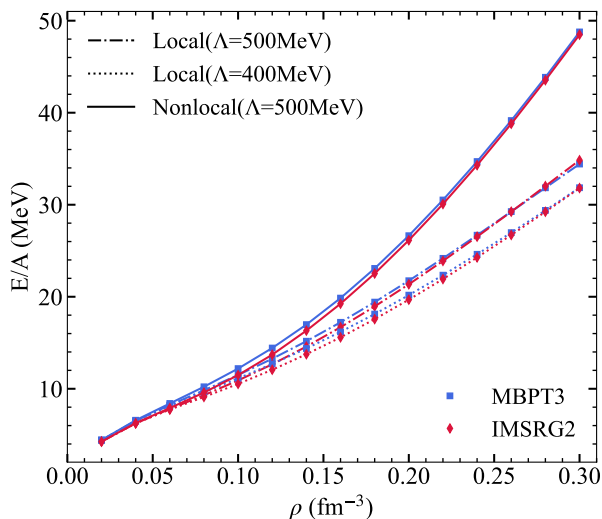


FIG. 5. Calculated energy per particle of pure neutron matter using NNLOopt plus different 3N forces. Results from MBPT3 and IMSRG(2) are compared. Calculations with different 3N nuclear forces with local and non-local regulators are shown, see text for details.

pendent on regulators. The local regulator is written as:

$$f_{\text{local}} = \prod_{j=1}^{N_j} \exp \left[ - \left( \frac{\mathbf{k}'_j - \mathbf{k}_j}{\Lambda_{3N}} \right)^{2n} \right]. \quad (26)$$

Here  $\mathbf{k}'_j - \mathbf{k}_j$  in the exponent factor denote transfer momentum and the index  $j$  sums over the transfer momentum of three nucleons. For the local regulator with a cutoff of 400 MeV, we adopt  $c_D=-0.39$  and  $c_E=-0.27$  ac-

cording to Ref. [23]. For a cutoff of 500 MeV, the parameters are taken as  $c_D = -0.39$  and  $c_E = -0.389$ . It is known that the contact terms have no contributions to neutron matter with a nonlocal regulator. It can be seen that the EoS with the nonlocal regulator is considerably harder than that with local regulators at higher densities. We see that MBPT3 results are slightly above IMSRG(2) in three calculations around the saturation density. However, MBPT3 becomes close to IMSRG(2) around two times of saturation density. Generally MBPT3 and IMSRG(2) results are close since the cutoff is not high.

## B. Symmetric Nuclear Matter

For pure neutron matter, we demonstrated that IMSRG(2) results are close to perturbative calculations, except for the nuclear interaction is harder with a cutoff of 700 MeV. It is interesting to study the difference between perturbative and non-perturbative calculations for symmetric nuclear matter. We adopt a local three-body regulator with a cutoff  $\Lambda=500$  MeV, together with NNLOopt to calculate the EoS of symmetric nuclear matter, as shown in Fig.6.

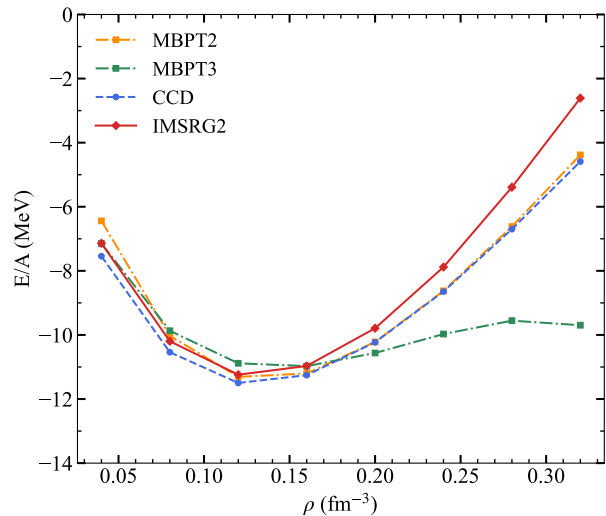


FIG. 6. Calculated energy per particle of symmetric nuclear matter using NNLOopt plus local 3N interactions ( $\Lambda=500$  MeV). Results from MBPT2, MBPT3, CCD and IMSRG(2) are compared.

Our calculations of symmetric nuclear matter agree well with earlier CCD results in [23]. We see that different methods have obvious discrepancies for symmetric nuclear matter. Indeed, symmetric nuclear matter is a strongly correlated system, while pure neutron matter is a relatively weakly correlated system [28]. Generally, MBPT2 results are relatively close to IMSRG(2) and CCD results. MBPT3 is significantly different from non-perturbative calculations above the saturation density. This indicates that MBPT3 is not enough for symmet-

ric nuclear matter at high densities. IMSRG(2) is above CCD and the difference becomes larger at higher densities. It has been pointed out that the residual three-body force has non-negligible effects for symmetric matter[23].

#### IV. DISCUSSIONS

In this work we have presented the development of the non-perturbative *ab initio* calculations of nuclear matter using In-Medium Similarity Renormalization Group method. IMSRG is a novel many-body method based on continuous unitary transformations to include infinite summation of MBPT diagrams. IMSRG method has been applied in studies of finite nuclei in the literature, but has not been used for infinite nuclear matter yet. Our code is built from scratch and have been benchmarked with coupled-cluster calculations. The present work IMSRG(2) has been adapted to use chiral two-body forces and three-body forces truncated at the normal-ordered two-body level.

The code enables calculations of IMSRG(2), MBPT to 4th order and CCD based on the same Hartree-Fock start. The calculations with different methods have been compared. The energy per particle from different methods are close for pure neutron matter using two-body forces NNLOopt, which is a soft interaction. In this case, MBPT4 is closer to IMSRG and CCD results compared to MBPT3. The situation is the similar for calculations

with three-body forces with a cutoff of 500 MeV. However, with a harder  $N^3LO$  nuclear force with a cutoff of 700 MeV, there is significant discrepancies between non-perturbative and perturbative calculations, in particular at higher density region. Furthermore, there is considerable discrepancies between different methods for symmetric nuclear matter even the nuclear interaction is soft. At the moment, our method is truncated at IMSRG(2) in the plane wave basis. It is costly to perform higher order IMSRG calculations such as IMSRG(3) and IMSRG(3f2), which have been realized recently for light nuclei [32, 33]. It is our next step to extend our calculations towards IMSRG(3) to use harder interactions, which should be insightful for studying EoS and short-range correlations at higher densities.

#### ACKNOWLEDGMENTS

We are grateful for useful discussions with B.S. Hu, W.G. Jiang. This work was supported by the National Key R&D Program of China (Grant No.2023YFE0101500, 2023YFA1606403, 2024YFA1610900), the National Natural Science Foundation of China under Grants No.12475118, 12335007, 12035001. We also acknowledge the funding support from the State Key Laboratory of Nuclear Physics and Technology, Peking University (No. NPT2023ZX01).

- 
- [1] A. L. Watts *et al.*, "Colloquium: Measuring the neutron star equation of state using x-ray timing," *Rev. Mod. Phys.* **88**, 021001 (2016).
  - [2] G. Burgio, H.-J. Schulze, I. Vidaña, and J.-B. Wei, "Neutron stars and the nuclear equation of state," *Prog. Part. Nucl. Phys.* **120**, 103879 (2021).
  - [3] L. Baiotti, "Gravitational waves from neutron star mergers and their relation to the nuclear equation of state," *Prog. Part. Nucl. Phys.* **109**, 103714 (2019).
  - [4] E. Annala, T. Gorda, E. Katerini, A. Kurkela, J. Nättilä, V. Paschalidis, and A. Vuorinen, "Multimessenger constraints for ultradense matter," *Phys. Rev. X* **12**, 011058 (2022).
  - [5] W. E. East, V. Paschalidis, F. Pretorius, and A. Tsokaros, "Binary neutron star mergers: Effects of spin and post-merger dynamics," *Phys. Rev. D* **100**, 124042 (2019).
  - [6] J. Bamber, A. Tsokaros, M. Ruiz, and S. L. Shapiro, "Post-merger gravitational wave signals from binary neutron stars: Effect of the magnetic field," *arXiv:2411.00943* (2024).
  - [7] S. Gandolfi, J. Carlson, S. Reddy, A. W. Steiner, and R. B. Wiringa, "The equation of state of neutron matter, symmetry energy and neutron star structure," *Eur. Phys. J. A* **50**, 10 (2014).
  - [8] K. Hebeler, J. M. Lattimer, C. J. Pethick, and A. Schwenk, "Constraints on neutron star radii based on chiral effective field theory interactions," *Phys. Rev. Lett.* **105**, 161102 (2010).
  - [9] R. W. Romani, D. Kandel, A. V. Filippenko, T. G. Brink, and W. Zheng, "Psr J0952-0607: The fastest and heaviest known galactic neutron star," *ApJL* **934**, L17 (2022).
  - [10] M. Chen, D. Guan, C. Jiang, and J. Pei, "Speed of sound and phase transitions in neutron stars indicated by the thick neutron skin of  $^{208}\text{Pb}$ ," *Phys. Rev. C* **108**, 065806 (2023).
  - [11] O. Komoltsev and A. Kurkela, "How perturbative QCD constrains the equation of state at neutron-star densities," *Phys. Rev. Lett.* **128**, 202701 (2022).
  - [12] S. Weinberg, "Nuclear forces from chiral Lagrangians," *Phys. Lett. B* **251**, 288 (1990).
  - [13] R. Machleidt and D. Entem, "Chiral effective field theory and nuclear forces," *Phys. Rept.* **503**, 1 (2011).
  - [14] R. Machleidt and F. Sammarruca, "Recent advances in chiral EFT based nuclear forces and their applications," *Prog. Part. Nucl. Phys.* **137**, 104117 (2024).
  - [15] H. Hergert, "A guided tour of *ab initio* nuclear many-body theory," *Front. in Phys.* **8**, 379 (2020).
  - [16] Q. Yuan, S. Q. Fan, B. S. Hu, J. G. Li, S. Zhang, S. M. Wang, Z. H. Sun, Y. Z. Ma, and F. R. Xu, "Deformed in-medium similarity renormalization group," *Phys. Rev. C* **105**, L061303 (2022).
  - [17] X.-Y. Xu, S.-Q. Fan, Q. Yuan, B.-S. Hu, J.-G. Li, S.-M. Wang, and F.-R. Xu, "Progress in *ab initio* in-medium similarity renormalization group and coupled-channel method with coupling to the continuum," *Nucl.*

- Sci. Tech.* **35**, 215 (2024).
- [18] K. Hebeler, "Three-nucleon forces: Implementation and applications to atomic nuclei and dense matter," *Phys. Rept.* **890**, 1 (2021).
- [19] L. Coraggio, J. W. Holt, N. Itaco, R. Machleidt, and F. Sammarruca, "Reduced regulator dependence of neutron-matter predictions with perturbative chiral interactions," *Phys. Rev. C* **87**, 014322 (2013).
- [20] C. Drischler, K. Hebeler, and A. Schwenk, "Chiral interactions up to next-to-next-to-next-to-leading order and nuclear saturation," *Phys. Rev. Lett.* **122**, 042501 (2019).
- [21] C. Drischler, R. J. Furnstahl, J. A. Melendez, and D. R. Phillips, "How well do we know the neutron-matter equation of state at the densities inside neutron stars? A Bayesian approach with correlated uncertainties," *Phys. Rev. Lett.* **125**, 202702 (2020).
- [22] G. Baardsen, A. Ekström, G. Hagen, and M. Hjorth-Jensen, "Coupled-cluster studies of infinite nuclear matter," *Phys. Rev. C* **88**, 054312 (2013).
- [23] G. Hagen, T. Papenbrock, A. Ekström, K. A. Wendt, G. Baardsen, S. Gandolfi, M. Hjorth-Jensen, and C. J. Horowitz, "Coupled-cluster calculations of nucleonic matter," *Phys. Rev. C* **89**, 014319 (2014).
- [24] M. Piarulli, I. Bombaci, D. Logoteta, A. Lovato, and R. B. Wiringa, "Benchmark calculations of pure neutron matter with realistic nucleon-nucleon interactions," *Phys. Rev. C* **101**, 045801 (2020).
- [25] P. Arthuis, C. Barbieri, F. Pederiva, and A. Roggero, "Quantum Monte Carlo calculations in configuration space with three-nucleon forces," *Phys. Rev. C* **107**, 044303 (2023).
- [26] A. Carbone, A. Rios, and A. Polls, "Correlated density-dependent chiral forces for infinite-matter calculations within the Green's function approach," *Phys. Rev. C* **90**, 054322 (2014).
- [27] A. Carbone, A. Polls, and A. Rios, "Symmetric nuclear matter with chiral three-nucleon forces in the self-consistent Green's functions approach," *Phys. Rev. C* **88**, 044302 (2013).
- [28] F. Marino, W. G. Jiang, and S. J. Novario, "Diagrammatic ab initio methods for infinite nuclear matter with modern chiral interactions," *Phys. Rev. C* **110**, 054322 (2024).
- [29] K. Tsukiyama, S. K. Bogner, and A. Schwenk, "In-medium similarity renormalization group for nuclei," *Phys. Rev. Lett.* **106**, 222502 (2011).
- [30] H. Hergert, S. K. Bogner, T. D. Morris, A. Schwenk, and K. Tsukiyama, "The in-medium similarity renormalization group: A novel ab initio method for nuclei," *Phys. Rept.* **621**, 165 (2016).
- [31] T. D. Morris, N. M. Parzuchowski, and S. K. Bogner, "Magnus expansion and in-medium similarity renormalization group," *Phys. Rev. C* **92**, 034331 (2015).
- [32] B. C. He and S. R. Stroberg, "Factorized approximation to the in-medium similarity renormalization group IM-SRG(3)," *Phys. Rev. C* **110**, 044317 (2024).
- [33] S. R. Stroberg, T. D. Morris, and B. C. He, "In-medium similarity renormalization group with flowing 3-body operators, and approximations thereof," *Phys. Rev. C* **110**, 044316 (2024).
- [34] A. Ekström, G. Baardsen, C. Forssén, G. Hagen, M. Hjorth-Jensen, G. R. Jansen, R. Machleidt, W. Nazarewicz, T. Papenbrock, J. Sarich, and S. M. Wild, "Optimized chiral nucleon-nucleon interaction at next-to-next-to-leading order," *Phys. Rev. Lett.* **110**, 192502 (2013).
- [35] D. R. Entem, N. Kaiser, R. Machleidt, and Y. Nosyk, "Peripheral nucleon-nucleon scattering at fifth order of chiral perturbation theory," *Phys. Rev. C* **91**, 014002 (2015).
- [36] D. R. Entem, R. Machleidt, and Y. Nosyk, "High-quality two-nucleon potentials up to fifth order of the chiral expansion," *Phys. Rev. C* **96**, 024004 (2017).
- [37] K. Hebeler and A. Schwenk, "Chiral three-nucleon forces and neutron matter," *Phys. Rev. C* **82**, 014314 (2010).
- [38] C. Drischler, *Nuclear matter from chiral effective field theory*, Ph.D. thesis, Technical University of Dortmund (2017).
- [39] R. Skibiński, J. Golak, K. Topolnicki, H. Witała, H. Kamada, W. Glöckle, and A. Nogga, "The Tucson-Melbourne three-nucleon force in the automatized partial-wave decomposition," *Eur. Phys. J. A* **47**, 48 (2011).
- [40] J. Golak, D. Rozpędzik, R. Skibiński, K. Topolnicki, H. Witała, W. Glöckle, A. Nogga, E. Epelbaum, H. Kamada, C. Elster, and I. Fachruddin, "A new way to perform partial-wave decompositions of few-nucleon forces," *Eur. Phys. J. A* **43**, 241 (2010).
- [41] M. Heinz, A. Tichai, J. Hoppe, K. Hebeler, and A. Schwenk, "In-medium similarity renormalization group with three-body operators," *Phys. Rev. C* **103**, 044318 (2021).
- [42] I. Shavitt and R. J. Bartlett, *Many-body Methods in Chemistry and Physics: MBPT and Coupled-Cluster Theory*, Cambridge University Press (2009).
- [43] P. Arthuis, T. Duguet, A. Tichai, R.-D. Lasserri, and J.-P. Ebran, "ADG: Automated generation and evaluation of many-body diagrams I. Bogoliubov many-body perturbation theory," *Comput. Phys. Comm.* **240**, 202 (2019).
- [44] M. Hjorth-Jensen, M. P. Lombardo, and U. Van Kolck, *An advanced course in computational nuclear physics, Springer Lecture Notes in Physics*, Vol. 936, Springer (2017).
- [45] D. R. Thompson, M. Lemere, and Y. C. Tang, "Systematic investigation of scattering problems with the resonating-group method," *Nucl. Phys. A* **286**, 53 (1977).
- [46] H. Y. Shang, R. Z. Hu, J. C. Pei, and F. R. Xu, "Properties of the chiral nucleon-nucleon interaction at N<sup>3</sup>LO with high cutoffs studied with a local projection approach," *Phys. Rev. C* **110**, 054003 (2024).